Discover Applied Sciences

Research

A novel energy harvesting technology from the movements of air masses

Carmelo Lodato[1] · Francesca Magionesi[2] · Giuseppe Marsala[3]

Received: 20 June 2024 / Accepted: 7 August 2024
Published online: 16 August 2024

Abstract
The displacement of air masses caused by the movement of objects or vehicles is often characterized by considerable energy content, which, with appropriate technologies, can be partially recovered. In this sense, numerous scientific works consider rail transport as a possible context for application. However, the literature in the sector highlights how using existing wind technologies in these areas involves many difficulties, mainly related to the turbulent and impulsive nature of the airflows generated. This work presents the architecture and general aspects of an innovative technology for obtaining electrical energy from variable and impulsive airflows, such as those due to the rapid transit of railway trains in tunnels, without precluding its use in other similar fields. The innovative aspect mainly concerns the independent control of two distinct typologies of bladed elements, which can also have translational movement and drag-based and lift-based aerodynamic behavior to improve the adaptability of the embodiment to the site's fluid dynamic and geometric characteristics. Furthermore, the structural simplification of the apparatus, shifting some of the technological complexity to the control systems, brings further advantages in terms of construction cost, robustness, maintenance, reuse, and transferability to different contexts. Of course, the counterpart of these benefits lies in the software and hardware of the control devices. Analytical models to determine the non-dimensional performance coefficients of the two basic types have been reported as has the architectural model of the control system. The technology shown in this work is protected by an EP and US Patent.

Keywords Energy harvesting · Wind power · Unconventional renewable sources · Railway · Road mobility

1 Introduction

In recent decades, the rapid increase in the population worldwide, the massive consumption of fossil energy, and their negative impact on the environment have triggered research efforts to find affordable and clean energies [1]. Specifically, energy harvesting has emerged as a pivotal process facilitating the capture of energy resources in diverse environments and subsequently converting them into electrical energy for immediate utilization or storage within dedicated devices. Railways, recognized as the most energy-efficient and sustainable form of transport for passengers and goods, are regarded as the core of transportation development in several countries, including China, Japan, and Germany. For instance, in China, the total length of railway lines reaches approximately 150,000 km [2, 3], with the high-speed section alone from Shanghai to Kunming including about 300 tunnels, covering a total length of over 400 km [4]. In this frame,

✉ Carmelo Lodato, carmelo.lodato@cnr.it | [1]CNR-ICAR: Istituto di calcolo e reti ad alte prestazioni, Via Ugo La Malfa 153, Palermo, Italy. [2]CNR-INM: Istituto di Ingegneria del Mare, Via di Vallerano 139, Rome, Italy. [3]CNR-INM: Istituto di Ingegneria del Mare, Via Ugo La Malfa 153, Palermo, Italy.

energy harvesting in the railway industry has great potential for energy recovery. In the technical literature, different approaches are explored; one of the most relevant focuses on using energy harvesting techniques exploiting vibrations of vehicle components (suspensions, shock absorbers, etc.) or induced by the interaction of the convoy with the railroad infrastructure (sleepers, joints, bridges, etc.) [5, 6]. The most common vibration energy harvesting systems for application in this context belong to the two following categories: electromagnetic and piezoelectric energy harvesters [7]. According to the previous literature, the vibrations usually involved in the railway's environment have a low amplitude (of the order of millimeters) and a wide frequency range (from a few tents to 6–7 hundred Herts). Electromagnetic devices [6] exhibit higher efficiency when displacement and frequency are high, whereas piezoelectric devices produce higher electricity when a significant strain is available to the harvesting system [8]. In particular, in [9], the vibrations detected at the track in a railway tunnel during a train passage can be fruitfully used to harvest energy. Most of these studies involve devices that typically utilize piezoelectric materials, which can provide useful power to supply moderately consuming auxiliary systems (of a few mW), such as onboard sensors for health-monitoring systems, wireless communications, signal lights, etc. For instance, in [10–12], the authors have developed piezoelectric devices capable of harnessing both the vibrations experienced by the train bogies and the wind induced by the train's movement. Despite the compact dimensions and the resulting low impact on structures or fluid dynamics in the environment, enabling the installation of multiple units, the use of these solutions remains specific to low-magnitude power. Other approaches in the scientific literature of the field are focused on utilizing solar energy [13]. The use of solar panels in rail transportation is not a novel concept; two different applications are presented in literature: those for which the solar panels are accommodated between the railroad lines and those for which the solar panels are located on the shed roof of each carriage. In a recent review [14], the authors reported applications of photovoltaic solar panels that generate up to 8% of the required power, mounting the panels on the roof of a diesel-electric train. Further studies in the scientific literature concern recovering higher powers from airflow [15] caused by the trains passing by resorting to conventional wind generators [16]. The increase in average train speed has opened up new possibilities for recovering energy from the airflow set in motion by passing trains. In particular, most of these studies focus on energy harvesting from small wind turbines installed either along the rail tracks or on the roofs of train wagons. In the former case, several patents have been proposed for generating renewable energy from moving trains by harnessing wind power. These studies encompass systems of both vertical-axis wind turbines (VAWT) (Savonius and Darrieus types) [17] and horizontal-axis wind turbines (HAWT). A singular prototype, as demonstrated by [18], is capable of producing energy in the range of a few tens of Watts. Assuming a number of systems per km equal to 250, the cumulative power output can potentially reach up to 3000 kWh/day/km. On the other hand, some critical aspects in the use of wind turbines positioned along the railroad arise from the frequent maintenance due to the potential vulnerability of the equipment to dust and debris raised during the train movement or to deposits of grease and dirt typical of the rail environment. Moreover, it is essential to note that installing small wind turbines within a tunnel poses safety concerns due to the presence of high-speed rotating devices. In [19], a modified Savonius-type VAWT microturbine installed in the space between tunnel walls and railway tracks is studied. The authors point out that the classical S-shape geometry of the blade does not allow for optimal electricity generation from induced wind, as the train passage creates a vortex near the turbine, with a low-pressure zone that hinders propeller blade rotation. The results indicate that although the developed modifications enhance its performance, they are susceptible to the blade diameter and the distance of the turbine from the tracks. In [20], the performance of a Banki-Michell turbine is investigated. The authors specify that traditional Savonius and Darrieus turbines, typically composed of two or three blades, are ill-suited for the substantial variations in airflow direction generated by the passage of a railway vehicle inside a tunnel, mainly due to the instability caused by the wide angle between the blades. The simulation, conducted by varying the number of turbines along the railway path and the length of the tunnel, reveals the performance dependency on the device's position relative to the train and the tunnel ends. In several studies, the rooftop of the train has been chosen for installing small wind turbines. This choice is motivated by high and consistent wind speed along long trails and the feasibility of installing the gearboxes and generators near the turbine. Technical literature presents several papers based on HAWT and VAWT [21]. In [22], the authors conduct a feasibility study on implementing a wind energy system composed of ten wind turbine units installed on the wagon roof, operating on different train routes (slow and fast). They found that the amount of power required to overcome the additional drag due to the presence of the wind turbines is almost 6% of the power requirement by the train. This result implies that the power output from a single trip is highly dependent on the mean velocity. Furthermore, considering the cost of the wind power unit, the payback time can be significantly increased for slow-route trains. Other significant limitations are associated with the placement of turbine systems on the train roof, including increased weight and dimensions [17]. These factors may restrict train entry into tunnels and pose additional challenges. A miniature wind energy harvester (MWEH) offers a new perspective on wind

power extraction. It can obtain power from aeroelastic instabilities, such as vortex-induced vibrations or flutter [23]. Their large-scale manufacturing feasibility and the possibility of generating motion at relatively low wind energy make this system particularly promising. Tunnel constitutes a highly distinctive infrastructure in terms of energy consumption and safety issues related to the high-risk level determined by the consequences of a potential risk event (fire, accident, etc.), as stated in Directive 2004/54/EC. Energy consumption linked to safety systems encompassing tunnel ventilation, traffic control, lighting, and communication is pivotal in achieving a sustainable design. In particular, with the rapid development of the information society, big data is a fundamental element in ensuring rail system's healthy and safe operation. In this frame, smart tunnels are implemented for measuring and collecting data from various parts of the equipment, which are further analyzed to ensure timely checking, identification of possible failures, and taking corrective measures. However, the increasing complexity of automation technical installations depends increasingly on reliable power supply. In particular, for tunnels situated in remote areas, electrical power supply to sensors and their maintenance becomes critical. Therefore, the research community has focused on energy harvesting methods in train tunnels. Within this context, energy harvesting through wind turbines can be effectively employed when the operational space and airflow characteristics associated with the aerodynamics of the tunnel and the vehicles passing through it align with the design specifications of the [19] wind device type. However, this condition is not easily encountered. In-depth analyses of the airflow in tunnels have highlighted the complexity of the aerodynamics occurring during the passage of vehicles, presenting numerous elements that hinder the efficient utilization of available energies. Various publications in the technical literature describe the interaction between flow, structures, and train [24–34]. The aerodynamic phenomenon triggered by the passage of a train through a tunnel is generally modeled by referencing two main aspects: the piston effect and the slipstream. The former primarily concerns the air pushed in front of the train and drawn in from the rear, while the latter involves the portion of air moving in the lateral space between the convoy and the tunnel. Specifically, compression waves are generated in the front region of the train and expansion waves in the rear area, both following the train's movement [34]. This scenario originates a complex pattern of air pressure and velocities along the tunnel's longitudinal direction and cross-section. The variability of the phenomenon depends, of course, on the geometric and physical characteristics of the train and the tunnel, as well as the speed of the train. A detailed analysis is provided in [24], revealing the significant airflow variability in flow rate, pressure gradient, turbulence, direction, duration, and position within the tunnel. The phenomenon's strongly impulsive and turbulent nature could also negatively affect structures and passengers, especially people waiting in designated areas. Further critical issues involve evaluating the impact of significant train-induced vibrations and the presence of debris, including high-speed propelled solid fragments. These factors pose potential threats to the integrity of facilities. So, to address these challenges, it is essential to make appropriate design choices that enhance the tolerance of infrastructures to such inconveniences. This work presents an innovative system for harnessing wind energy induced by the passage of vehicles in railway or subway tunnels. The primary objective is to provide a technology capable of enhancing the adaptability of equipment to the specific fluid dynamic characteristics of these operational contexts while also increasing performance levels compared to existing technologies. Improved adaptability to the site's geometry offers the additional advantage of extending airflow control strategies, for example, to exert a solicited braking action or reduce undesired effects on passengers waiting near the track. The technology presented in this work is protected by an EP and US Application Patent [35]. The rest of the paper is organized as follows. In Sect. 2, the technological background provides an overview of the leading reference technologies. Section 3 describes the main apparatus component's overall architecture and functional aspects. Section 4 shows the essential algebra for determining the dimensionless performance coefficients and two embodiment examples reported in the patent. An overview of the system controller model is described in Sect. 5. Finally, Sect. 6 reports considerations and future works.

2 Background

The key features of the technological background are presented here to facilitate comprehension of the developed technology, emphasizing its primary challenges in application in the chosen context (railroad tunnel). A simplified description of the main elements encompassing the developed system is described hereafter: wind turbines, electrical generators, and control systems.

2.1 Wind turbines

Although the complexity of aerodynamic phenomena inside a railway tunnel significantly changes the efficiency of conventional wind turbines in this operational context, a brief description of the process of converting wind energy into electrical energy is reported below. The amount of power P extracted by the wind turbine is a fraction of the power P_f of the air mass impacting it, which can be expressed by the well-known formula [36]:

$$P_f = 1/2\rho A v_f^3 \tag{1}$$

where ρ is the air density, A is the swept area, and v_f is the wind velocity. The extracted power can be related to the available power in the airflow by the non-dimensional power coefficient C_p according to the following expression:

$$P = P_f \cdot C_p \tag{2}$$

The theoretical maximum efficiency of a wind turbine in aerodynamic-mechanical conversion is determined by Betz's limit [37]. The well-known Betz's model, as outlined in [38], is based on the axial momentum theory and employs the concept of actuator disk [39] to model a generic wind turbine, analyzing the volume of an ideal fluid constituted by the flow tube that passes through a porous disk. The power coefficient C_p of a generic wind apparatus is expressed as follows:

$$C_p = P/\left(1/2\rho A v_f^3\right) = (1-a)^2 4a \tag{3}$$

It depends on the axial interference factor a that quantifies the interaction between the flow and the device. The axial interference factor is defined as the ratio of the decrease in airflow velocity in front of the actuator disc v to that of the undisturbed flow:

$$a = \left(v_f - v\right)/v_f \tag{4}$$

It is demonstrated that the wind speed on the actuator disc v is equal to the average of the velocities at the inlet v_f and outlet v_u of the flow tube:

$$v = \left(v_f + v_u\right)/2 \tag{5}$$

Then, the axial interference factor cannot exceed the value 0.5, corresponding to $v_u = 0$, i.e., flow interruption. The maximum power coefficient $C_p = 16/27$, obtained with $a = 1/3$, gives the theoretical efficiency limit of 59.26%. However, C_p is usually less than 45%. This significant reduction in the power coefficient is due to aerodynamic losses in the wind turbine systems.

2.2 Electric generators

The mechanical rotational energy of a turbine's rotor axis is converted into electrical energy through an electric generator. In traditional wind turbines, most drive systems incorporate a gearbox and a high-speed induction generator. However, as wind turbine's average power has significantly increased, there is a growing interest in direct-drive low-speed generators, with attention to some technical and economic constraints. A wind turbine can be either at fixed or variable speed type. The former is aerodynamically less efficient, operating optimally only at a specific wind speed, but has been widely adopted due to its reliability, simplicity, and low costs. The latter adapts to wind speed, optimizing energy extraction in an extensive range of velocities. Usually, fixed-speed wind turbines use a mechanical multi-stage gearbox to drive a high-speed induction generator [40]. A wind turbine operating at a variable speed can be characterized by a doubly fed induction generator (DFIG) or a permanent magnet synchronous generator (PMSG) [20]. The PMSGs present advantages for direct-drive wind turbines by eliminating gearbox compared to asynchronous induction machines. In particular, the electrical excitation is replaced by permanent magnets, which minimizes rotor-winding losses and decreases generator weight. Moreover, because the PMSG does not need a gearbox, slip rings, and brushes, they are characterized by high reliability and low maintenance cost [20, 40]. Electro-mechanical conversion is a highly efficient process that can be over 90% using permanent magnet synchronous generators. PMSG is one of the most efficient types of generators. Indeed, it does not need extra electrical power and is characterized by a small, light, and robust structure [17]. In particular, the

power losses of this type of generator are about 65% of those of a typical DFIG [41]. In [42], the authors propose the design and development of a PMSG generator for small-scale wind turbines subjected to turbulent wind. In particular, the generator-inverter system described can be used as an active technique for controlling turbine speed in strong winds. In high-wind operating conditions, an extra electrical dump load can slow down the turbine if the wind speed exceeds a prefixed threshold. The excess electrical energy is diverted to this dump load, dissipating it as heat. This load essentially acts as a brake for the turbine, preventing it from spinning too fast. When the wind speed drops or returns to a safe range, the dump load can be disconnected, allowing the turbine to accelerate again. Various approaches have been utilized in moving train's wind energy harvesting systems. In tunnels, wind speeds can vary significantly and change rapidly. To ensure a more stable rotation of the wind turbine, a brushed DC motor as the generator seems to be the better choice. In [22] and [43], the generator unit used is a PMSG. It does not require additional capacitors for power factor corrections, even if it demands high maintenance and frequent repair work due to the presence of brushes coupled with a gearbox to regulate the shaft rotational speed. In, [12, 44, 45], the authors justify the use of a microturbine with a PMSG generator because of the high variability of the wind speed caused by the fast dynamic of the phenomena that produce the airflow inside the tunnel. In [17], the authors use a PMSG generator installed on a train roof because it does not require wiring for excitation. Also, this solution allows for satisfying the constraints of the proposed apparatus's weight.

2.3 Control systems

Control strategies in wind energy systems are crucial for optimizing their performance, efficiency, and reliability. These strategies aim to address the inherent challenges associated with wind variability, turbulence, and grid integration, ensuring that the turbine operates correctly in varying conditions while maintaining structural integrity and maximizing energy capture [46]. Usually, the operating range of a wind turbine is defined by the cut-in and cut-out wind speed values. Below the cut-in, the available energy does not compensate for operational costs and transmission losses. At the same time, above the cut-out, the turbine is subjected to high mechanical loads that may cause damage. Within the turbine's operating range, different control methods are applied. Traditionally, in the so-called full load region (i.e., at high wind speed), the control strategy object is to ensure the safe and stable operation of the turbine by keeping the generated power and rotor speed close to the rated value. These strategies are based on blade pitch control or stall control [47–49]. These methods enable the turbine to modulate the aerodynamic forces on the blades and, consequently, the aerodynamic torque applied to the rotor, optimizing power extraction and mitigating mechanical stress during high wind speeds. The difference between pitch control and stall control is mostly noticeable under high wind speed conditions: stall-controlled systems rely on the aerodynamic design of the blades to ensure the control of the aerodynamic torque or rotational speed of the turbine in high wind speed conditions, whereas pitch-controlled systems employ active pitch control mechanisms for the blades. An advanced pitch control strategy is the IPC (individual pitch control), where the control strategy adjusts the pitch angle of each blade independently. This allows for finer control and optimization of the blade's aerodynamic performance, providing suppression of the fluctuations of blade flapwise moments and also a reaction of the tower loads and drivetrain loads, particularly in response to wind turbulence. Stall control is a low-cost technique with respect to the pitch-controlled system since it does not require the installation of actuators. Nevertheless, it exhibits decreased efficiency under low wind speeds, and it causes fluctuations in maximum steady-state power. For small wind turbines, a commonly applied control strategy is based on the horizontal furling method, whereby turning the blades away from the wind direction as the wind speed increases beyond a specific limit. Therefore, it causes the effective wind speed to decrease on the rotor plane, thus lowering the aerodynamic power of the wind turbine. The controller aims to maximize power production in the low wind speed region, i.e., the so-called partial load region. In this region, a generator torque controller is usually used to change the rotational speed to obtain an optimal tip speed ratio. Even though wind turbines often behave strongly as nonlinear systems, stemming from the complexity of their structure and the stochastic nature of wind speed, many researchers have employed linear system theory directly. These approaches are based on linearization techniques to get the mathematical model of a wind turbine near the selected fixed operating point, and the control law is then designed based on the linearized model. A detailed review of power regulation control techniques can be found in [50, 51]. Typical implementation approaches are structured according to a hierarchical decomposition, decomposing the control systems into more manageable, interrelated tasks requiring less data. Proportional integral derivative (PID) controllers adjust the pitch angle based on the error between the desired and actual values, considering the proportional, integral, and derivative terms. PID controllers are the most commonly used and are also effective in maintaining stability and regulating the turbine's response to changing wind conditions. The nonlinear nature of the dynamics of wind turbines required tuning with trial and error procedures. Other linear

control strategies are the feedback control and state-space control [47]. While, linear control theory has been widely used in wind turbine control, its limitations in handling nonlinearities, uncertainties, and system complexity have led to the development of more advanced nonlinear control techniques tailored to the specific challenges of wind turbine control. Several nonlinear control strategies have been developed; these include fuzzy control, sliding mode neural network control [52, 53], and nonlinear PID control. Moreover, Genetic Algorithms (GAs) are metaheuristic algorithms commonly used for pitch angle controllers in WT systems. These controllers aim to ensure system stability during low wind speed conditions, allowing for the maximal extraction of wind power by adjusting the pitch angle based on the available wind speed. Finally, equally crucial is the role of the control system in a wind farm, where it is necessary to implement cooperation strategies oriented towards the appropriate distribution of the electrical load required by the grid among the available turbines. Attention is paid to prevent a turbine from causing harmful airflow interference that powers the others, minimizing turbulence and wake effects [54, 55].

3 Technology architecture

The block diagram in Fig. 1 provides an introductory representation of the presented technology, including the main structural elements and functional aspects. The apparatus comprises two wind energy systems (WES – wind energy system), each with a single-bladed device (BD-bladed device).

The apparatus interacts with the airflow via the blades of each bladed device. A generic embodiment must include at least one BD with one blade element (BE). The BE is constrained to move cyclically along a pre-established trajectory composed of one or more oriented segments. At least one active phase must be present when the flow exerts a proper force on the blade. The passive phases concern the motion of the blade in trajectory segments where the movement does not produce work. Active phases, in turn, can differ in the aerodynamic action, drag/lift exerted by the airflow on the blade. Variations in the orientation and trajectory of the blade with respect to the direction of the airflow hitting

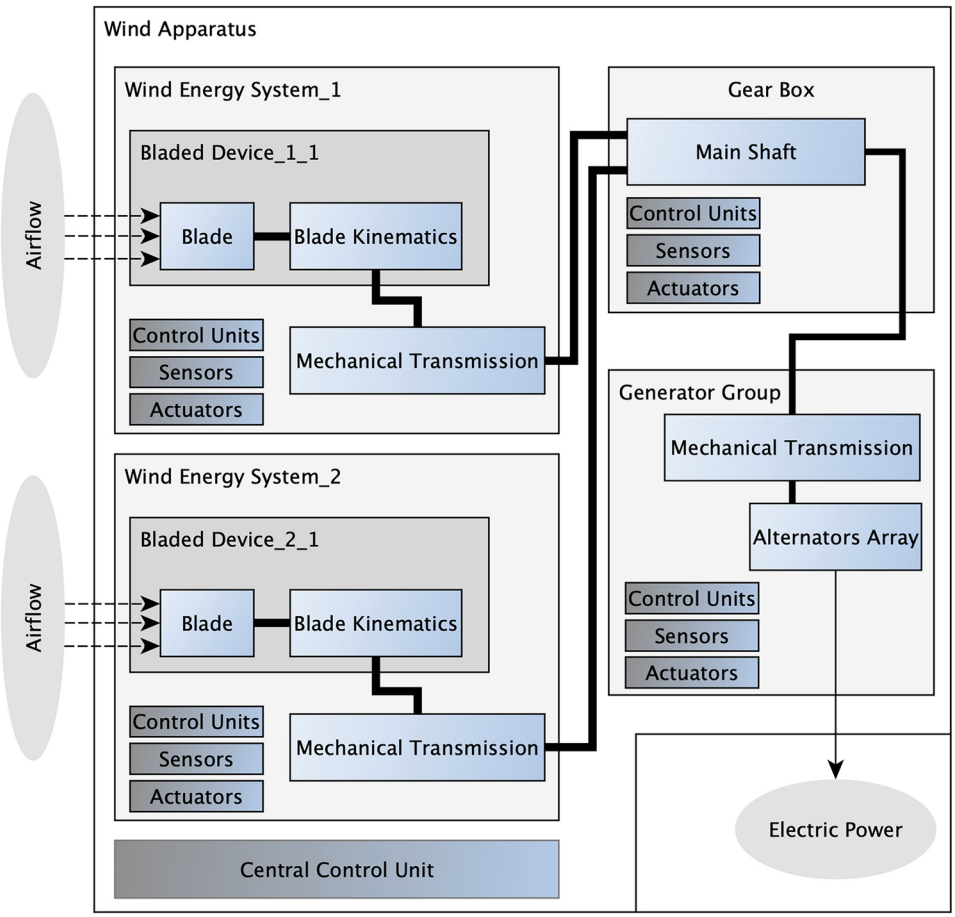

Fig. 1 Basic architectural model of the apparatus

it modify the aerodynamic behavior of the device. These variations can concern the whole blade or a specific portion thereof. They can be implemented by specific actuators, controlled by control units, based on data (positional, kinematic, dynamic, and fluid dynamics) provided by specific sensors, and processed by a control unit. Therefore, by varying these parameters, a BD can adopt an aerodynamic configuration that is more sensitive to drag force (Drag-based configuration) or lift force (Lift-based). Suitable kinematics transform the blade's cyclic motion into a shaft rotation. The power is transferred to the Gear Box block through mechanical transmission and, therefore, to the primary rotational shaft inside it. This transmission box, equipped with electronically controlled electromechanical systems, can vary the transmission ratios to optimally combine the contribution of each wind energy system and transfer the mechanical power to the group of generators. The generator group, including single or multiple rotary or linear alternator units, converts mechanical energy into electrical energy. Mechanisms similar to the previous ones, when necessary, connect and/or disconnect one or more units. Finally, data transmission systems (not highlighted in the figure) ensure the appropriate exchange of information and commands among the different units, including sensors external to the device, and with the central control unit to manage the system components, regulate their operation and synchronism, and provide interfacing with any external devices. The following sections outline the general principles of both subsystems, primarily based on the drag effect and those based on the lift effect.

3.1 Drag-based system configuration

Figure 2 shows the schematic representation of a wind energy system comprising two bladed devices, each equipped with a Drag-based bladed element. This scheme is a minimal example of device geometry without limiting the technology's potential, thus allowing flexibility in configuring the system according to the specific installation site requirements. In this configuration, the two BEs have rectilinear trajectories positioned horizontally. Each BE comprises two equal parts placed symmetrically with respect to the travel axis, which can rotate with respect to a horizontal axis located between them and orthogonal to the direction of movement. The configuration of the BE can be modified based on the information provided by position and/or inertial sensors, for example, through electromechanical devices controlled by the central control unit's software.

The BE in the foreground in Fig. 2 has a flat surface exposed to the wind's action. It is placed orthogonally to the prevailing airflow direction, which is represented horizontally and directed towards the right, to maximize the aerodynamic resistance against the flow. In this case, the element is in the active phase because, being hit by the airflow, a thrust is exerted on it, just as happens on a vessel sailing with a tailwind (downwind) [56]. The thrust intensity depends on the flow characteristics, orientation, geometry, and direction of movement of the BE, specifically on the aerodynamic drag coefficient C_D of the element. The other BE, depicted in the background, is in the passive phase. It can be observed that the two parts are closed like a book, causing the BE to assume a configuration of minimum aerodynamic resistance in its direction of advancement, which, as shown by the blue arrow, is opposite to that of the wind (cyan arrows) and is due to the dragging action exerted by the BE in the active phase. As shown in Fig. 2, constructing the BE with two distinct parts can reduce the bladed device's overall size while maintaining the same exploitable surface area. The two-bladed elements come to touch each other along their respective strokes without interfering because the element in the passive phase passes through the gap between the two parts of the one in the active phase. Reducing the operating space

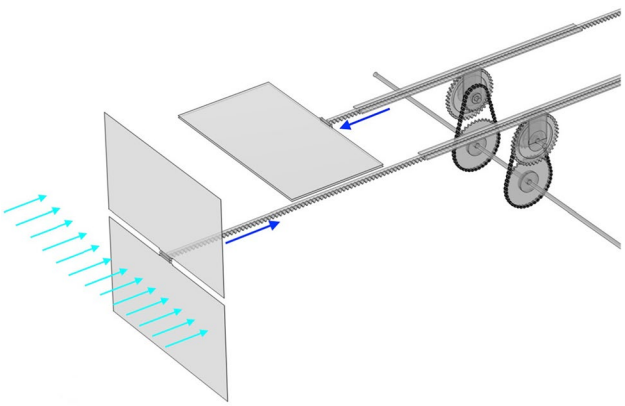

Fig. 2 Drag-based bladed device

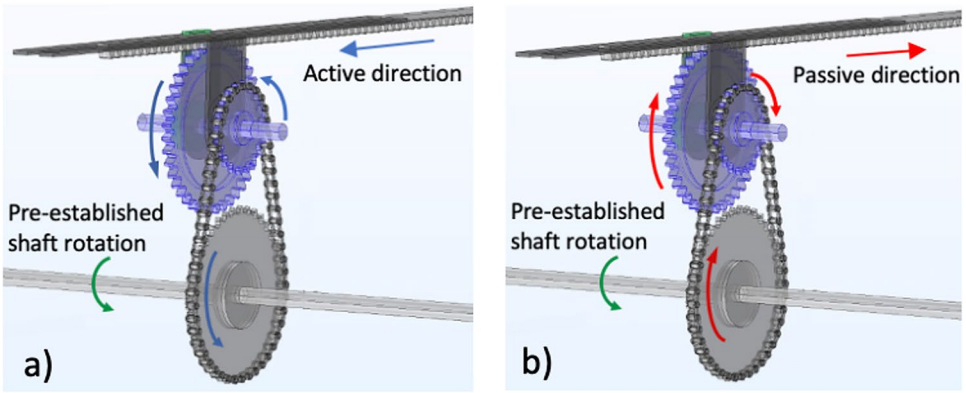

Fig. 3 Schematic configuration of the single-acting freewheel

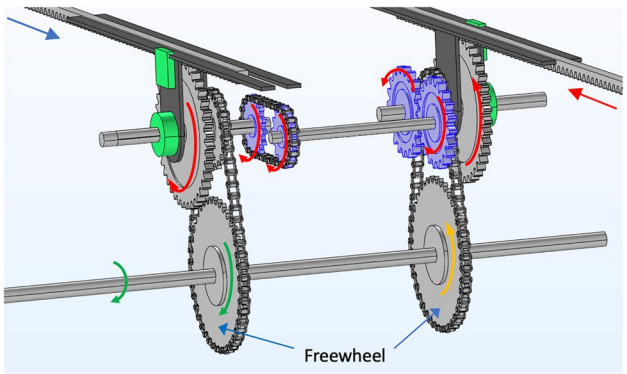

Fig. 4 Example of BDs mechanical transmission with BEs synchronization system

through appropriate geometries and arrangements of the BEs can represent an advantage compared to conventional rotating systems.

Finally, Fig. 3a and b show a possible mechanical configuration for converting the alternating translational movement of the BEs into a pre-established shaft rotation direction. The mechanism includes a rack for each bladed element, with a length adequate to the maximum expected stroke, integrated with the BE, and capable of sliding on a guide. The rack is coupled to a pinion, and through additional gears, its motion is transmitted to a freewheel pulley [57] that transfers only the torque concordant with the pre-established direction of shaft rotation while rotating in neutral in the opposite direction. This configuration lends itself to using linear alternators, allowing for further simplification of the mechanical system for transmitting motion to the group of generators.

The dragging of one BE by the action of another implies the control of synchronism and a connection between the BEs, ensured, for example, by a connection mechanism like the one represented in Fig. 4 with a chain (or a belt) and pulley system. The BE on the left is in the active phase and moves in opposite directions to the BE on the right. However, it is reiterated that the descriptions reported are only schematic and have conceptual value; they do not represent optimized construction choices from an engineering point of view.

3.2 Lift-based system configuration

The schematic WES in Fig. 5 illustrates a bladed device, including a lift-based BE. The blade element can move up and down along the straight vertical guide in this example. The BE comprises movable components that allow the shape and orientation of the airfoil to be varied. As in the previous case, the airflow is horizontal and oriented to the right. The two configurations assumed by the BE correspond to an asymmetric profile arranged to generate a positive (Fig. 5a) or negative lift (Fig. 5b), respectively. Therefore, both oriented segments that make up the cyclical trajectory of the BE represent active phases.

As for the previous drag-based case, the BE's configuration can be realized with electromechanical devices controlled by the central control unit's software based on the information provided by positional and/or inertial sensors. According

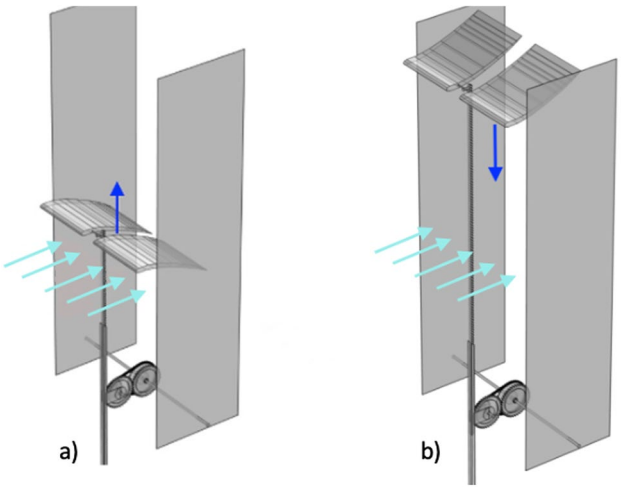

Fig. 5 Lift-based bladed device

to the nautical analogy, the drag-based and lift-based cases correspond to the downwind and abeam speed (reach/upwind for inclined trajectory segment).

The system, therefore, exhibits different aerodynamic behavior when the shape, orientation, and direction of movement of the BE varies with respect to the direction of the airflow. Also, in this double-acting configuration, a rack system similar to the previous one can be considered for converting the translational movement of the BEs into the movement of a rotational shaft. A schematic depiction of the mechanism is presented in Fig. 6. However, two freewheel gears are keyed onto the rotating shaft, with coaxial ones on the right. They transmit only clockwise torque to their common axis and rotate freely (in neutral) in an anticlockwise direction. Each of the two series of colored arrows indicates the movement of the gears that cause the shaft rotation, specifically the cylindrical gear and the chain ones (placed in the background), for each direction of movement of the rack.

4 Governing equations

This section describes the mathematical modeling essential to determine the dynamic effects that an airflow, characterized by density ρ and reference velocity of the undisturbed flow v_f, can exert on the active parts of the two BD types (drag and lift) and to allow a way to evaluate the general performance of each device.

4.1 Drag-based

The wind energy system shown in Fig. 2 consists of two single-acting bladed devices $N_{BD} = 2$, each including one bladed element, synchronized with a 180° phase shift in the operating cycle. In this configuration, the wind energy system always

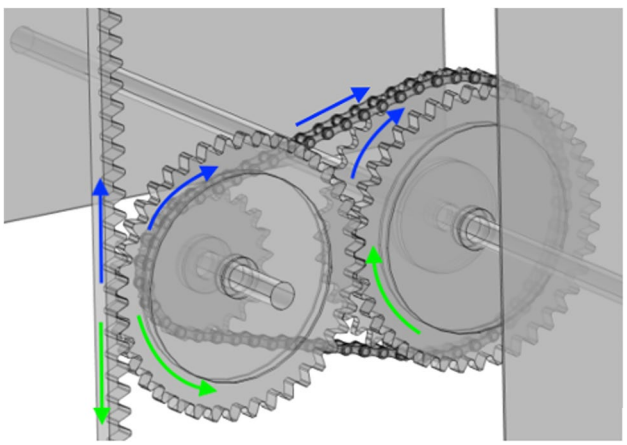

Fig. 6 Schematic configuration of the double-acting freewheel

maintains only one BE in the active phase. It is well known that the total force F_D in the direction of motion exerted by a fluid in motion at a velocity v_f on a generic structure is given by:

$$F_D = C_D \frac{1}{2} \rho S v_f^2 \tag{6}$$

where C_D is the aerodynamic resistance coefficient and S is the area of the orthographic projection of the structure on a plane perpendicular to the direction of motion. When the structure is in motion, the relative velocity between it and the fluid must be considered. In this case, since the structure is moving in the same direction as the flow, the relative velocity varies only in amplitude, decreasing its value. Therefore, indicating with N_{BE} the number of bladed elements in the active phase of the cycle, the thrust that the flow exerts on a wind energy system of the type depicted in Fig. 7 is given by:

$$F_D = C_D \frac{1}{2} \rho N_{BE} S_{BE} v_f^2 \left(1 - \alpha_D\right)^2 \tag{7}$$

where C_D is the drag coefficient of the BE configured for the active phase, S_{BE} is the reference section of each bladed element, given by the projection of the surface of the BE in the active phase on the plane orthogonal to the direction of the airflow, and α_D is the speed ratio defined as the ratio between the average speed v_{BE} of the BE in the active phase and that of the undisturbed flow:

$$\alpha_D = \frac{v_{BE}}{v_f} \tag{8}$$

The developed power $P_D = F_D \times v_{BE}$ is given by:

$$P_D = C_D \frac{1}{2} \rho N_{BE} S_{BE} v_f^3 \alpha_D \left(1 - \alpha_D\right)^2 \tag{9}$$

Solidity σ can be defined analogously to wind turbines as the ratio to the bladed area and the overall surfaces occupied by the BEs:

$$\sigma = \frac{S_x}{A_x} \tag{10}$$

where S_x is the projection onto the plane orthogonal to the airflow direction of the overall surface S of the N_{BE} bladed elements, whereas A_x is the projection of the surface A of all the bladed elements, considering them in an open configuration, that is when they occupy the maximum space. The solidity σ of the device depends on the specific geometry of the BEs and the respective kinematics of the BD. In the case of Fig. 7 (flag arrangement), neglecting the size of the guide elements, the BEs in the open configuration are entirely superimposed. Therefore, surface A coincides with the surface in active phase S of the BEs, giving rise to $\sigma = 1$. In the configuration of Fig. 2, $\sigma = 2/3$ because the BEs overlap is equal to 1/2. However, for side-by-side BEs, where there is no overlap, $\sigma = 1/2$. It can be noticed that for the present configuration, the maximum value of solidity is one, and decreasing σ reduces the space's efficiency. For this wind energy system (Fig. 7) it is:

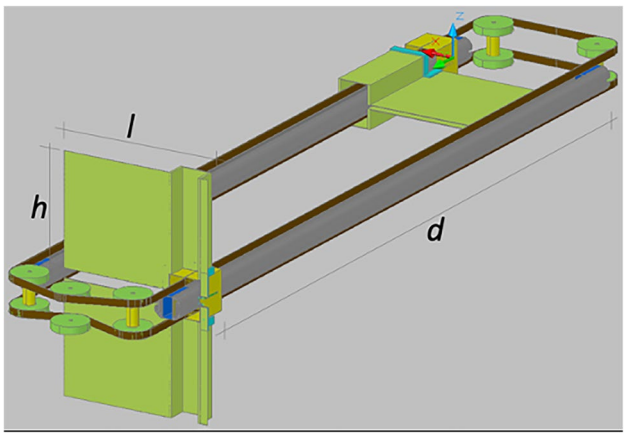

Fig. 7 Drag-based wind energy system

$$S_x = N_{BE}\ S_{BE} \tag{11}$$

and substituting (11) into (10), we obtain the analytical expression of the reference surface area A_x to calculate the performance non-dimensional coefficients:

$$A_x = \frac{N_{BE} \cdot S_{BE}}{\sigma} \tag{12}$$

Therefore, by dividing the Eqs. (7) and (9) respectively by the reference values of force and the power of the fluid, given by $F_f = {}^1/_2 \rho A_x v_f^2$ and $P_f = {}^1/_2 \rho A_x v_f^3$, the dimensionless thrust and power coefficients are:

$$C_s = C_D\, \sigma \left(1 - \alpha_D\right)^2 \tag{13}$$

$$C_p = C_D\, \sigma\, \alpha_D \left(1 - \alpha_D\right)^2 \tag{14}$$

In Fig. 8, the curves of the thrust and power dimensionless coefficients as a function of the relative speed ratio α_D of the bladed element are depicted considering the drag coefficient $C_D = 1.0$. The solidity σ has been chosen equal to 1.0, neglecting the spatial dimensions of the guide elements and the gap between the two parts of BEs. This drag-based wind energy system is characterized by a thrust that assumes maximum value $C_D \cdot \sigma$ when the BE is motionless and progressively decreases as the relative speed increases. By setting the derivative of Eq. (14) with respect to α_D equal to zero, with simple algebraic steps, the value of the relative speed coefficient corresponding to the maximum power is determined:

$$\alpha_D\left(P_{max}\right) = \frac{1}{3} \tag{15}$$

The corresponding known values of the thrust and power coefficients, as for Savonius wind turbines, are:

$$C_s\left(\alpha_D{=}1/3\right) = \frac{4}{9}\, C_D\, \sigma \tag{16}$$

$$C_p(\alpha_D{=}1/3) = \frac{4}{27}\, C_D\, \sigma \tag{17}$$

4.2 Lift-based

The wind energy system shown in Fig. 5 consists of a single-bladed device ($N_{BD} = 1$), including a bladed element ($N_{BE} = 1$) oscillating alternately along the y-axis, orthogonal to the indicated airflow direction. The system configuration enables

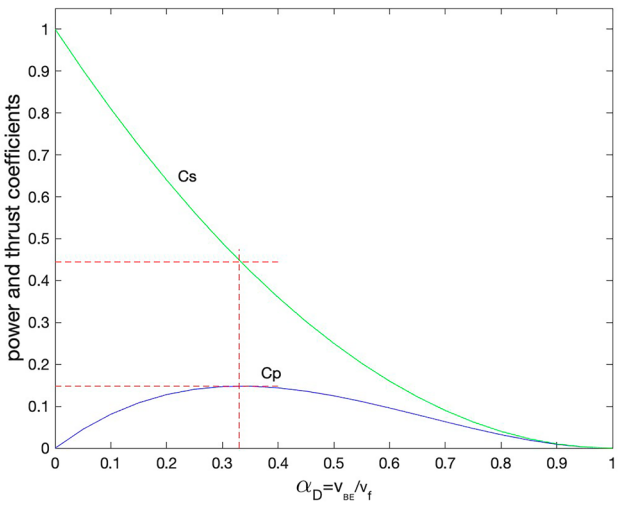

Fig. 8 Non dimensional power and thrust curves as a function of speed ratio α_D

active phase in both upward and downward directions by exploiting the positive and negative lift. This capability is achieved through a variation in the wing geometry, as described in the "Lift-based system configuration" section. When a generic structure moves in a direction different from that of the flow impacting it, the relative flow velocity varies in magnitude and direction, significantly differentiating the dynamic behavior of the lift-based system as compared to the drag one. Figure 9 depicts the velocity triangle for the bladed element of the lift-based device when it moves upward (in the positive y direction) with a velocity V_y and is subjected to the aerodynamic action of an airflow acting in the x direction with velocity V_f. From Fig. 9, it is evident that the apparent velocity v_A and the angle between the apparent velocity and the undisturbed fluid velocity can be expressed as follows:

$$v_A = \sqrt{v_f^2 + v_y^2} \quad \tan\beta = \frac{v_y}{v_f} \tag{18}$$

Moreover, the following force components are obtained:

$$F_y = F_{Ly} - F_{Dy} \tag{19}$$

$$F_x = F_{Lx} + F_{Dx} \tag{20}$$

with:

$$F_L = \frac{1}{2}\rho S v_A^2 C_L \tag{21}$$

$$F_D = \frac{1}{2}\rho S v_A^2 C_D \tag{22}$$

The forces exerted on the BE (19, 20) can be rewritten as:

$$F_y = \frac{1}{2}\rho S v_A^2 \left(C_L \cos\beta - C_D \sin\beta\right) \tag{23}$$

$$F_x = \frac{1}{2}\rho S v_A^2 \left(C_L \sin\beta + C_D \cos\beta\right) \tag{24}$$

As for the drag-based device, it is possible to define a speed ratio as the ratio between the average speed of the BE and that of the undisturbed flow:

$$\alpha_L = \frac{v_y}{v_f} \tag{25}$$

By combining the Eqs. (18) and (25), the following expressions are obtained:

$$v_A = \sqrt{v_f^2\left(1 + \alpha_L^2\right)} \quad \tan\beta = \alpha_L \tag{26}$$

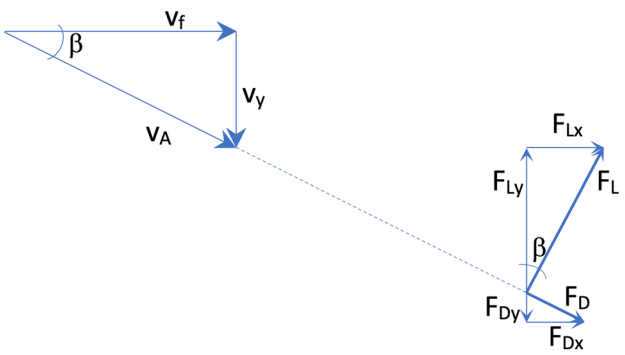

Fig. 9 Velocity triangle for lift-based device

and the components (23, 24) of the forces acting on the BE can be rewritten using the Eqs. (26):

$$F_y = \frac{1}{2}\rho N_{BE} S_{BE} v_f^2 \sqrt{1+\alpha_L^2}\left[C_{L\theta} - C_{D\theta}\alpha_L\right] \tag{27}$$

$$F_x = \frac{1}{2}\rho N_{BE} S_{BE} v_f^2 \sqrt{1+\alpha_L^2}\left[C_{L\theta}\alpha_L + C_{D\theta}\right] \tag{28}$$

where $C_{D\theta}$ e $C_{L\theta}$ represent the drag and lift aerodynamic coefficients of the BE airfoil section for a predetermined angle of attack θ. S_{BE} denotes the reference section of the BE, equal to the product of the wingspan *l* and the chord *c*.

The Betz model has been considered to account for the mutual interaction between the airflow and the wind energy device. This model introduces the axial interference factor *a* Eq. (4). The following known relations, obtained by balancing the axial moment, provide thrust and power extractable from a turbine with a rotor of section *A* as a function of the axial interference factor:

$$T = 2\rho A v_f^2\, a(1-a) \tag{29}$$

$$P = 2\rho A v_f^3\, a(1-a)^2 \tag{30}$$

and from Eq. (30) derives the well-known maximum value of the power coefficient $C_p = 16/27$ (Betz limit), which sets a limit on the percentage of theoretically extractable power from the airflow that passes through the actuator disk, achieved at an axial interference value of $a = 1/3$, as mentioned in the "Background" section. Similar considerations can be applied to the wind energy system under study. To consider the effects of the interference exerted by the wind energy device on the fluid, by considering the horizontal fluid's speed $(1-a)v_f$ in the velocity triangle of Fig. 9, the Eqs. (26) become:

$$v_A = \sqrt{v_f^2\left[(1-\mathrm{a})^2 + \alpha_L^2\right]} \quad \tan\beta = \frac{\alpha_L}{1-a} \tag{31}$$

Therefore, considering the interference induced by the bladed device on the airflow that passes through it, the previous relations (27) and (28) of the vertical and horizontal components of the forces acting on the BE are:

$$F_y = \frac{1}{2}\rho N_{BE} S_{BE} v_f^2 \sqrt{(1-a)^2+\alpha_L^2}\left[C_{L\theta}(1-a) - C_{D\theta}\alpha_L\right] \tag{32}$$

$$F_x = \frac{1}{2}\rho N_{BE} S_{BE} v_f^2 \sqrt{(1-a)^2+\alpha_L^2}\left[C_{L\theta}\alpha_L + C_{D\theta}(1-a)\right] \tag{33}$$

For the calculation of the thrust and power coefficients, considering Eqs. (32, 25) and taking as reference the force F_f and the power P_f (previously defined) of the fluid crossing the surface A (given by the product of the wingspan *l* and the stroke *d*) swept by the BE in its cycle, it is obtained:

$$C_s = \frac{N_{BE} c}{d}\sqrt{(1-a)^2+\alpha_L^2}\left[C_{L\theta}(1-a) - C_{D\theta}\alpha_L\right] \tag{34}$$

$$C_p = \frac{N_{BE} c}{d}\sqrt{(1-a)^2+\alpha_L^2}\,\alpha_L\left[C_{L\theta}(1-a) - C_{D\theta}\alpha_L\right] \tag{35}$$

Here, in analogy to the rotor wind turbines, the solidity σ is defined as the ratio of the blade area to that swept by the blades:

$$\sigma = \frac{N_{BE}\, c}{d} \tag{36}$$

and the non-dimensional performance coefficients can be rewritten as follows:

$$C_s = \sigma\sqrt{(1-a)^2+\alpha_L^2}\left[C_{L\theta}(1-a) - C_{D\theta}\alpha_L\right] \tag{37}$$

$$C_p = \sigma\sqrt{(1-a)^2+\alpha_L^2}\alpha_L\left[C_{L\theta}(1-a) - C_{D\theta}\alpha_L\right] \tag{38}$$

By imposing the equality between the horizontal component F_x of the aerodynamic action on the BE and the thrust T, respectively expressed by the Eqs. (29, 33), assuming the incoming surface $A = l \cdot d$ and tacking in account Eq. (36), the following expression for the numerical calculation of the axial interference factor a relating to the lift-based wind energy system is obtained:

$$a_{i+1} = \frac{\sigma}{4}\frac{\sqrt{(1-a_i)^2+\alpha_L^2}\quad\left[C_{L\theta}\alpha_L + C_{D\theta}(1-a_i)\right]}{1-a_i} \tag{39}$$

From the Eqs. (37–39), it is possible to obtain the values of the thrust coefficient, the power coefficient, and the axial interference as a function of the relative speed ratio α_L for the lift-type wind energy system. Figure 10 refers to non-dimensional coefficients for a case with BE aerodynamic efficiency equal to 10 ($C_{D\theta} = 0.1, C_{L\theta} = 1.0$). It includes the trust and power curves for solidity $\sigma = 0.25$ ($N_{BE} = 1, c = 0.25, d = 1$) and $\sigma = 0.33$ ($c = 0.33$). The plot highlights how varying the overall bladed surface or stroke of the BEs can change both the specific power and the relative speed corresponding to the maximum point.

4.3 A drag-lift coupled system configuration

This section briefly describes two embodiments included in the patent application. The two types of wind energy systems, i.e., drag- and lift-based, exhibit significantly different performance characteristics and optimal operating points, as highlighted in the "Drag-based" and "Lift-based" sections. Their peculiarity can be effectively used to enhance power capture from airflow by suitably integrating the two different devices into a single wind energy system. This approach offers significant advantages across various structural and functional aspects. For instance, it enables the adoption of the device shapes and dimensions according to the geometric characteristics of the installation site. Similarly, in terms of fluid dynamics aspects, it enables tuning the contribution of the two wind energy systems (i.e., lift- and drag-based) to optimize performance and enhance operational stability.

As depicted in Fig. 1, the two wind systems can be integrated into a single device through appropriate variable ratio motion transmission mechanisms to optimize the contributions. Figure 11 shows a basic implementation of an integrated wind turbine system composed of two WES.

A drag-based system is installed in the lower part of the apparatus, composed of two single-acting BD with horizontal stroke and a 180° phase difference. Above it, a lift-based energy system is positioned, comprising a single BD configured

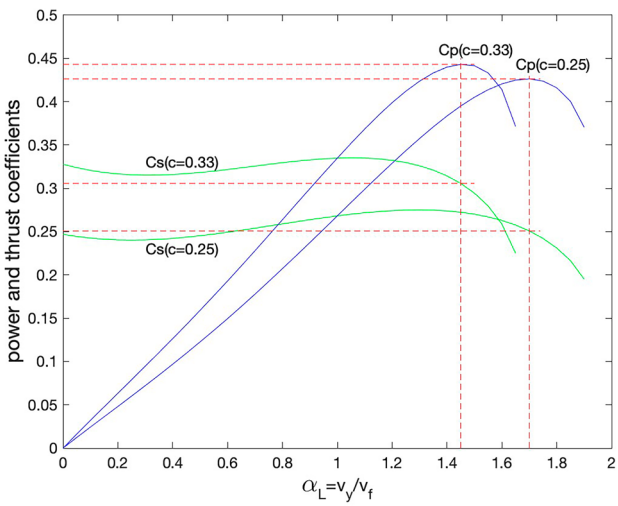

Fig. 10 Non dimensional power and thrust curves as a function of speed ratio α_L

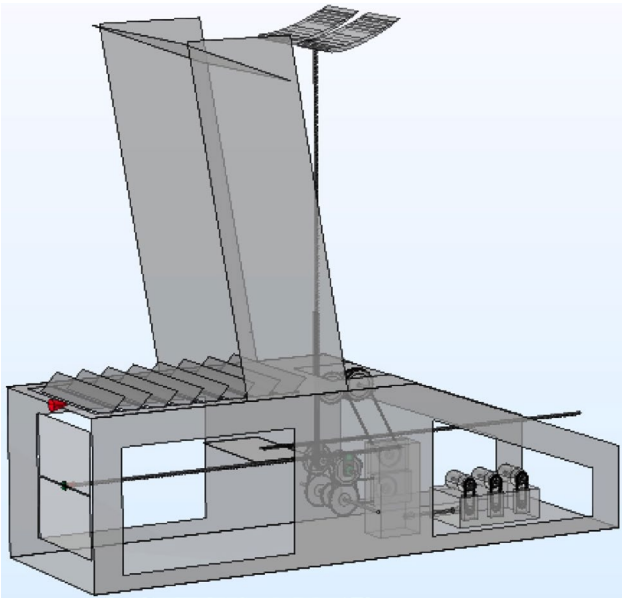

Fig. 11 A generic integrated wind energy apparatus

with one double-acting BE and vertical stroke. The cross-section of the blade element, as depicted in Fig. 5, is represented as an airfoil that can be configured for positive and negative lift, enabling the active phase in both upward and downward directions.

For explanatory purposes only, to provide an order of magnitude of the performances obtainable with an installation in a realistic railway context, calculating the maximum predictable power based on the governing equations described in Sects. 4.1 and 4.2 is reported here, considering a stable airflow. Since the speed range of trains, from subway routes to long-distance railway lines, is extensive, $v_f = 15$ m/s is assumed.

Table 1 summarizes the essential parameters for a general configuration and sizing of the type of apparatus shown in Fig. 11.

For the mechanical to electrical conversion, a permanent magnet alternator capable of delivering a power of 500 W with a voltage of 400 V, with a nominal speed of 400–4200 [rpm] and characterized by an efficiency $\eta \geq 0.9$ was considered.

A detailed discussion is the subject of future work. Here, it is specified that, in the calculation, a variable mechanical ratio has been considered for the drag-based device to maintain the relative speed $\alpha_D \leq 1/3$. The graph in Fig. 12 shows

Table 1 Main characteristics of a realistic wind energy apparatus

Lift-based wind energy system	
Profile	NACA 0012
Angle of attack	10°
Drag coefficient	0.019
Lift coefficient	1.04
Span	1 m
Chord	0.4 m
Stroke	2 m
Number of blade elements	3
Drag based wind energy system	
Drag coefficient	1.169
Length of the blade element	1 m
Height of the half-blade element	0.3 m
Hinge joint gap blade element	0.02 m
Stroke	2 m
Number of blade elements	1

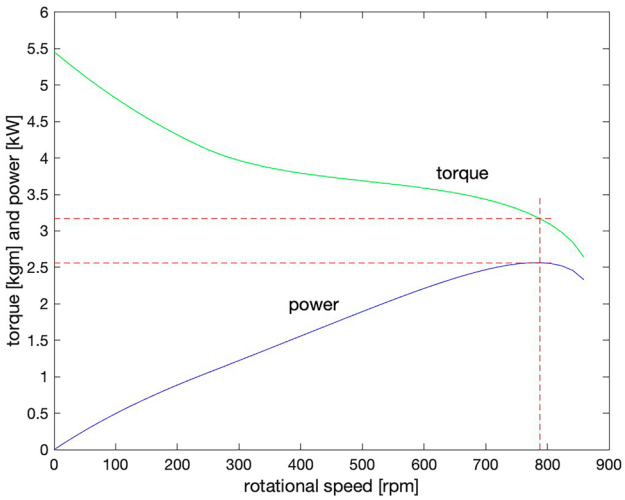

Fig. 12 Torque and power diagram for drag-lift coupled apparatus

the torque and power curves at the final shaft as a function of the rotation speed in rpm. With the contribution of the drag-based device, the maximum torque is 5.46 kgm and, at a speed of 400 rpm it is 3.78 kgm. The power exceeds 1.5 kW at 400 rpm. The maximum power is 2.56 kW at 788 rpm, and the corresponding torque is 3.17 kgm.

The mechanical torque necessary for the alternator's start-up is derived from its technical specifications. In the specific case, at the maximum power regime, four units can start with an electrical power production of 2 kW.

Figure 13 shows a possible embodiment of an integrated wind energy system designed explicitly for employment in a railway tunnel or underground line. While the base form of this apparatus's drag-based WES, designed explicitly for railway tunnels, does not substantially vary, the lift-based WES differs. It includes two BDs, each composed of a series of BEs whose stroke follows a curved trajectory dictated by the tunnel geometry. In both cases depicted in Figs. 11 and 13, the bladed devices of the two wind energy systems are interconnected and linked through the terminal transmission shaft to the group of generators using suitable electronically controlled variable ratio motion transmission mechanisms.

These mechanisms can dynamically regulate the device interaction and transmit the motion to electric generators based on the available instantaneous power. As mentioned, the strategy described entails transferring a portion of complexity from the structural aspects to the control aspects, both constructively and operationally, as described in the following section.

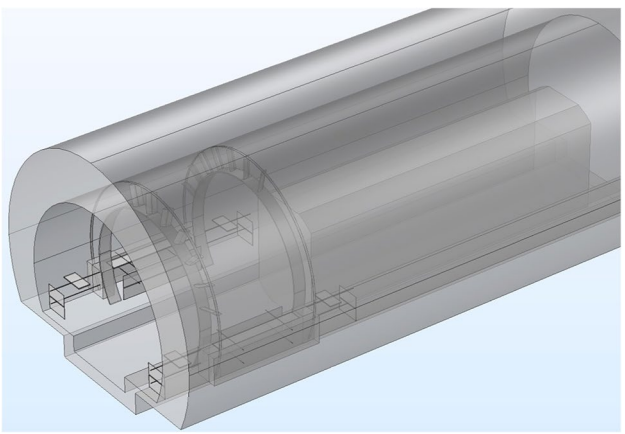

Fig. 13 Integrated wind energy embodiment for railway tunnel

5 Controller modeling overview

The complexity of the aerodynamic phenomenon, especially in the transient regime, and the heterogeneous characteristics of the two types of BEs (drag- and lift-based) give the control system a key role in the wind energy apparatus. To achieve synergistic management of the multiple and different WESs of the described apparatus, a more complex control model is required compared to conventional wind turbines. At the level of a single WES, the control system must provide many of the typical functions of wind turbine software and additional functionalities essential for the proper operation of components specific to the present apparatus. A typical function also present in the control of conventional turbines is, for example, the dynamic correction of the angle of the BE with respect to the incident wind and the speed of the single BE to maximize the extracted power. Among the functions specific to the present apparatus are procedures for regulating the speed or frequency of movement of bladed elements when the variability of the airflow requires it. Another function, not specifically for efficiency purposes, is activating particular conditions such as the aerodynamic brake or the airflow redirecting. At the global level, the control system must act similarly to what happens in Wind Farms, orchestrating all subsystems to obtain a coordinated behavior. In a wind farm, the control implements cooperation strategies for appropriate load distribution, minimizing turbulence and wake effects that could cause harmful airflow interferences. Here, instead, an essential task of global control is to distribute, when necessary, the mechanical power between the WESs of the apparatus, especially for optimizing and managing start-up and shut-down in response to environmental and operating conditions. It must also guarantee efficiency, robustness, and operational safety under various circumstances that may occur in the operational context. From an architectural point of view, the control system has been defined according to a multilevel hierarchical model typically used for wind turbines, where intricate procedures are decomposed into more manageable tasks requiring less data, however integrating the additional functional blocks essential for the present technology. The overall structure of the control system is presented below without describing the strategies that implement the various functional blocks, which will be addressed in future works. The developed control model, depicted in Fig. 14, is modular and scalable, consistent with the architecture of the apparatus shown in Fig. 1. Going into a more detailed description, the model comprises several sub-units, each dedicated to a specific device,

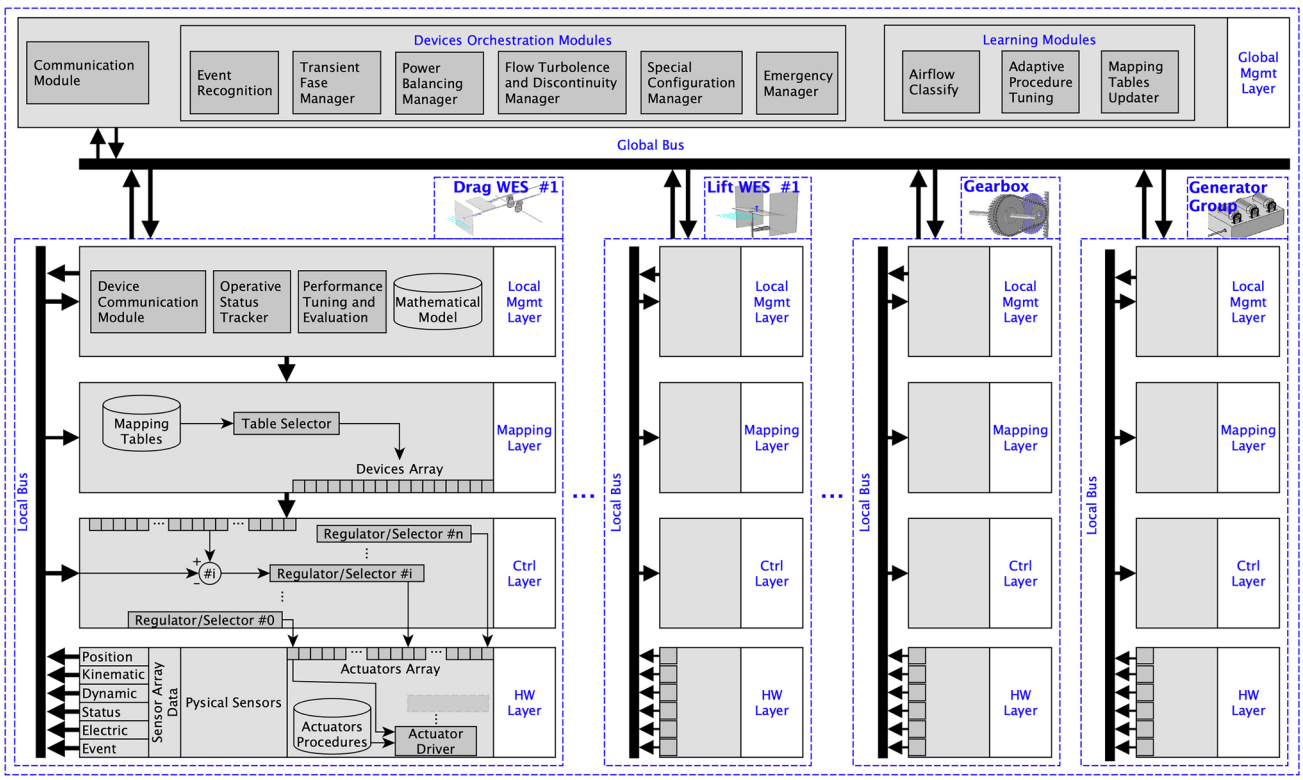

Fig. 14 Control model of the apparatus

including each WES, a gearbox, a group of electric generators, and above them, a supervisory control block named Global Management Layer (GML). From the bottom, each sub-unit is organized into four levels: Hardware, Control, Mapping, and Local Management. The system's sensors and actuators are located at the hardware level of each block. This layer includes the procedures for interpreting the sensor data, which are classified according to the type of information they provide. A transversal communication bus (Local Bus) makes these data available to the other levels. The actuators act based on the commands that the higher level (Control Level) issues, according to an appropriate coding, in dedicated storage areas. The Control Level implements all the functional units responsible for regulating monitored parameters and tracking the optimal reference points while stabilizing the actuators at the underlying Hardware Level. For instance, this level manages tasks such as adjusting the instantaneous gear ratio of the gearbox or adapting the generator configuration in response to the airflow force on the BE, the BE velocity, and the instantaneous power produced by the WES. The Mapping Level contains dedicated storage for Mapping Tables, structured to provide the desired regulation parameters in quantized form at the lower level, depending on the instantaneous operating conditions. Overseeing an individual block, such as a WES, the Gearbox, or the Generator Group, falls under the purview of the Local Management Level. For example, within a WES block, this layer implements strategies for instantaneously regulating the blade angle of attack to achieve the desired dynamic regime and maintain optimal performance based on the device's current state and the theoretical model. The Local Management Level may also incorporate functionalities such as Operative Status Tracker, and Performance Tuning and Evaluation, which are algorithms responsible for controlling the system's dynamics in the various phases of each bladed device's operating cycle.

Coordinating all the block components of the Wind Apparatus is the responsibility of the Global Management Layer.

It also acts on the gearbox and the generators, balancing each WES's contributions to satisfy the prescribed performance according to the implemented strategies. Through the global transmission bus and the communication modules, the GLM receives parameters on the airflow, information on the dynamics of the devices, and the operational status of the various components of the apparatus. So, it can recognize and classify the type of event performing, for example, associations between airflow patterns, convoy type, and relative state of motion. With this information, GML regulates both transient and steady-state operation of the Wind Apparatus, trying to bring and maintain each WES in its operating region using the Power Balancer. This procedure can request power from one device, release it to another WES, or modify the performance target of a WES. Specifically, the Power Balancing Manager queries each WES's Performance Tuning and Evaluation, determining whether and how to redistribute the power. With said cooperation strategy, for instance, in the presence of airflow events characterized by pronounced impulsiveness, by exploiting the differences in the response of each bladed device to the fluid dynamic stress, part of the power captured by a device instead of being transmitted to the generator can advantageously be redirected towards another bladed device. If efficiently implemented, this approach could overcome instability events and quickly bring each bladed device to its nominal operating speed, maintaining it for longer. This procedure is also carried out in case of anomalous airflow variations or emergencies, with parameters and methodologies tailored by the pertinent managers. Finally, advanced predictive and adaptive control strategies could be located at this level.

6 Discussion and conclusion

Rail transport infrastructure is constantly increasing, as is the frequency of trips in the subways of large urban centers. Furthermore, there will likely be further growth in using these infrastructures for different reasons linked, such as reducing emissions and consumption, at least concerning private mobility. Therefore, the transit of convoys, specifically in tunnels, represents a scenario of concrete interest in the field of energy recovery both for the number of potential sites for the installation of the systems and for the theoretically available powers, which in the technical literature are estimated in the order of megawatts per kilometer. On the other hand, the growth in the frequency of trips and the consequent increase in the average speed of the convoys leads to greater consumption both in terms of energy and the wear and tear of the vehicles. Furthermore, it is necessary to keep the effects of induced wind within acceptable limits, generally on the technical installations but above all on passengers. Based on the theoretical model prepared, this work's considerations show how the technology presented can adapt to the variability and impulsiveness of the airflow specific to this context. The characteristic of the two drag/lift-based subsystems of reacting differently to the same wind stress, as well as the possibility of sizing them differently and measuring their contribution independently, can increase the adaptability of the wind energy system to the specific fluid dynamics and geometry of the installation site, improving efficiency even in transient operation, naturally, by arranging

adequate software control, for example, to match the movement frequency of the bladed elements to that of the flow that solicits them. Furthermore, the choice to also use translating elements, therefore both continuous and alternating cycle movement trajectories, can provide further advantages, such as facilitating compact configurations of the devices by reducing the overall dimensions of the apparatus and increasing specific performances. An aspect already described is the transfer of a share of complexity from the structural part to the control part, both in terms of systemic and operation. The advantage of this choice is twofold. On the one hand, different structural characteristics of distinct types of wind turbines can be parameterized to make them dynamically activated and, if necessary, arrange them in a single device. Secondly, the lower complexity of the structural part offers the possibility of reducing the design and construction costs of the apparatus. The resulting more complex control system can be managed with today's high-performance technologies of processing, sensors, and actuator devices, as well as adaptive and predictive software based on AI techniques.

The technology presented is scalable and modular, and the railway tunnel context may present the opportunity to create multiple installations. However, it is not generally possible to quantify the number of installations per unit length of the railway route because the choice of positioning an apparatus depends on some essential considerations. One of these concerns the speeds of trains, which can vary significantly at different points of a tunnel, consequently varying the available flow power. Another aspect concerns the action that the device exerts during its operation on the flow, which can cause harmful interference with other nearby devices. The spaces available in the sections of a tunnel can vary considerably for various reasons, such as structural, for the installation of infrastructure, or reasons related to technical regulations. This aspect may prevent the implementation on a specific site or require a new design and sizing of the device.

In any case, each device, regardless of its size, is equipped with the electronic peripherals (sensors, actuators, controllers) necessary for its operation, including devices for transforming mechanical energy into electrical energy. Sensors external to the apparatus and arranged along the tunnel, for example, for measurements of wind speed and pressure or for identifying the type of convoy, can be used to evaluate the type of event and improve the regulation of the apparatus. Apart from these sensors, no additional peripherals are necessary in case of multiple installations of the device.

To provide an order of magnitude of the maximum achievable power, the performance values and a torque/power graph as a function of the rotation speed have been presented for a realistically sized apparatus. The example shown concerns a basic configuration susceptible to large margins for improvement. However, we would like to clarify here that the performance values have been provided to allow a comparison with conventional wind technologies. An evaluation consistent with the hypotheses described and appropriate to the chosen operational context cannot ignore the analysis of a specific case. In fact, to quantify the actual power extracted from a device it is necessary to at least evaluate the number of energy events as well as the duration and intensity of each of them. Therefore, it is necessary to know the frequency of train passages, the lengths of the trains, and their speed at the site of the apparatus. Of course, adequate fluid dynamic studies are also essential to maximize the captured power and evaluate and control the mutual interactions and are the focus of a future article.

Based on a conservative approach, it is possible to take the auxiliary devices used on small turbines as a reference. Microcontrollers commonly used for implementing control systems, such as the Arduino, STM32 Nucleo, and Raspberry Pi, typically consume power within a range that does not exceed a few watts. Usually, the current and voltage sensors have low power consumption, typically of a few milliwatts each, whereas power and energy meters range from a few hundred milliwatts to a couple of watts. Anemometers consume similar power, depending on the type. For the specific case, instead of hydraulic actuators, electrical ones are usually applied, which require between 10 to 100 watts, depending on the aerodynamic load and the size of the blades. It is essential to underline that the actual power consumption is lower than nominal power because it is calculated by the PWM signal's duty cycle. As a result, the power of the auxiliary devices is considered in the order of a few tens of watts.

Finally, only a feasibility study on a specific case can evaluate the actual economic feasibility of an installation in the specified context, considering the real operating cycles.

Due to its structural characteristics, the technology reduces construction, operation, and maintenance costs compared to conventional technologies. On the other hand, additional upfront costs exist for designing each piece of equipment. The cost of the control part, including the software, has a reasonably low impact because it is designed to be modular and configurable on different devices. However, the task of tuning the device takes on greater importance.

In conclusion, further advantages that the technology provides concern the possibility of appropriately directing part of the airflow caused by vehicles moving in the tunnel. In this way, for example, the annoying and sometimes dangerous effects for people waiting at stations can be mitigated. Flow direction control can be used, where required, to exert an aerodynamic slowing action on the convoy, reducing wear on the braking system.

Besides being of interest to the community in terms of a more environmentally friendly public mobility service, the proposed technology can be attractive for public administrations and any companies involved in managing and maintaining the viability of infrastructures considered. Future research activities include calculating the performance of an apparatus designed for a specific site and evaluating the system's efficiency at predetermined fluid dynamic stresses.

Author contributions C.L.: Conceptualized the work and drafted all sections of the manuscript, preparing all figures. Individual contribution concerns the Sect. 4*. G.M.: Contributed to Sects. 3*, 5 and 6. F.M. and G.M.: Contributed to Sects. 1, 2*, and References. All authors reviewed the manuscript.

Funding No funding was received for conducting this study.

Data availability The authors declare that the data supporting the findings of this study are available within the paper, and supplementary information related to the application patent is publicly available as follows. Italian application patent: https://www.uibm.gov.it/bancadati/Number_search/type_url?type=wpn with id-number 102022000019611 European application patent: https://register.epo.org/application?number=EP23198712 United States application patent: https://ppubs.uspto.gov/dirsearch-public/print/downloadPdf/20240102451.

Declarations

Competing interests The authors declare that they have no competing interests.

References

1. UN, General Assembly. Transforming our world: the 2030 Agenda for Sustainable Development. A/RES/70/1. (2015). From: https://www.refworld.org/docid/57b6e3e44.html
2. Xu W, Zhou J, Qiu G. China's high-speed rail network construction and planning over time: a network analysis. J Transp Geogr. 2018;70:40–54.
3. Liu W, Lund H, Mathiesen BV. Modelling the transport system in China and evaluating the current strategies towards the sustainable transport development. Energy Policy. 2013;58:347–57.
4. Fu M, Li P, Liang XF. Numerical analysis of the slipstream development around a high-speed train in a double-track tunnel. PLoS ONE. 2017;12(3): e0175044.
5. Romero A, Cámara-Molina JC, Moliner E, Galvín P, Martínez-Rodrigo MD. Energy harvesting analysis in railway bridges: an approach based on modal decomposition. Mech Syst Signal Process. 2021;160: 107848.
6. Pan Y, Zuo L, Ahmadian M. A half-wave electromagnetic energy-harvesting tie towards safe and intelligent rail transportation. Appl Energy. 2022;313: 118844.
7. Qi L, Pan H, Pan Y, Luo D, Yan J, Zhang Z. A review of vibration energy harvesting in rail transportation field. iScience. 2022;25(3): 103849.
8. Duarte F, Ferreira A. Energy harvesting on railway tracks: state-of-the-art. Proceed Institut Civil Eng-Transp. 2017;170(3):123–30.
9. Wischke M, Masur M, Kröner M, Woias P. Vibration harvesting in traffic tunnels to power wireless sensor nodes. Smart Mater Struct. 2011;20(8): 085014.
10. Jin L, Deng W, Su Y, Xu Z, Meng H, Wang B, et al. Self-powered wireless smart sensor based on maglev porous nanogenerator for train monitoring system. Nano Energy. 2017;38:185–92.
11. Cho JY, Jeong S, Jabbar H, Song Y, Ahn JH, Kim JH, et al. Piezoelectric energy harvesting system with magnetic pendulum movement for self-powered safety sensor of trains. Sens Actuat A: Phys. 2016;250:210–8.
12. Zheng P, Qi L, Sun M, Luo D, Zhang Z. A novel wind energy harvesting system with hybrid mechanism for self-powered applications in subway tunnels. Energy. 2021;227: 120446.
13. Hao D, Zhang T, Guo L, Feng Y, Zhang Z, Yuan Y. A high-efficiency, portable solar anergy-harvesting system on a foldable-wings mechanism for self-powered applications in railways. Energ Technol. 2021;9(4):2000794.
14. Fayad A, Ibrahim H, Ilinca A, Karganroudi SS, Issa M. Energy efficiency improvement of diesel-electric trains using solar energy: a feasibility study. Appl Sci. 2022;12(12):5869.
15. Nakayama Y. Introduction to fluid mechanics. Oxford: Butterworth-Heinemann; 2018.
16. Rao KR. Wind energy for power generation: meeting the challenge of practical implementation. Berlin: Springer; 2019.
17. Hyman M, Ali MH. A novel model for wind turbines on trains. Energies. 2022;15(20):7629.
18. Raja Sekhar Y, Natarajan M, Chiranjeevi C, Sukanta R, Yugandhar P. Experimental study on vertical axis wind turbine to harness wind power from rapidly moving railway locomotives. In: Theoretical, computational, and experimental solutions to thermo-fluid systems: select proceedings of ICITFES 2020. Springer Singapore, pp. 445–450 (2021)

19. Bethi RV, Laws P, Kumar P, Mitra S. Modified Savonius wind turbine for harvesting wind energy from trains moving in tunnels. Renew Energy. 2019;135:1056–63.
20. Verde A, Lastres O, Hernández G, Ibañez G, Verea L, Sebastian PJ. A new method for characterization of small capacity wind turbines with permanent magnet synchronous generator: an experimental study. Heliyon. 2018;4(8):00732.
21. Sindhuja B. A proposal for implementation of wind energy harvesting system in trains. In: Proceedings of the 2014 international conference on control, instrumentation, energy and communication (CIEC). IEEE (2014) (pp. 696–702).
22. Nurmanova V, Bagheri M, Phung T, Panda SK. Feasibility study on wind energy harvesting system implementation in moving trains. Electr Eng. 2018;100:1837–45.
23. Wen Q, He X, Lu Z, Streiter R, Otto T. A comprehensive review of miniatured wind energy harvesters. Nano Mater Sci. 2021;3(2):170–85.
24. Niu J, Sui Y, Yu Q, Cao X, Yuan Y. Aerodynamics of railway train/tunnel system: a review of recent research. Energy Built Environ. 2020;1(4):351–75.
25. Raghunathan RS, Kim HD, Setoguchi T. Aerodynamics of high-speed railway train. Prog Aerosp Sci. 2002;38(6–7):469–514.
26. Ku YC, Rho JH, Yun SH, Kwak MH, Kim KH, Kwon HB, Lee DH. Optimal cross-sectional area distribution of a high-speed train nose to minimize the tunnel micro-pressure wave. Struct Multidiscip Optim. 2010;42:965–76.
27. Wang F, Liu F, Han J, Jin H, Weng M, Zeng Z. Study on the train-induced unsteady airflow in a metro tunnel with multi-trains. Tunn Undergr Space Technol. 2020;106: 103565.
28. Liu TH, Chen XD, Li WH, Xie TZ, Chen ZW. Field study on the interior pressure variations in high-speed trains passing through tunnels of different lengths. J Wind Eng Ind Aerodyn. 2017;169:54–66.
29. Howe MS, Winslow A, Iida M, Fukuda T. Rapid calculation of the compression wave generated by a train entering a tunnel with a vented hood: short hoods. J Sound Vib. 2008;311(1–2):254–68.
30. Yan X, Tao L, Peng J, Zeng Y, Fang Y, Bai Y. Behavior of piston wind induced by braking train in a tunnel. Energies. 2020;13(23):6420.
31. Khayrullina A, Blocken B, Janssen W, Straathof J. CFD simulation of train aerodynamics: train-induced wind conditions at an underground railroad passenger platform. J Wind Eng Ind Aerodyn. 2015;139:100–10.
32. Rocchi D, Tomasini G, Schito P, Somaschini C. Wind effects induced by high speed train pass-by in open air. J Wind Eng Ind Aerodyn. 2018;173:279–88.
33. Moreno T, Pérez N, Reche C, Martins V, De Miguel E, Capdevila M, et al. Subway platform air quality: assessing the influences of tunnel ventilation, train piston effect and station design. Atmosph Environ. 2014;92:461–8.
34. Pan S, Fan L, Liu J, Xie J, Sun Y, Cui N, et al. A review of the piston effect in subway stations. Adv Mech Eng. 2013;5:950205.
35. Lodato C, Marsala G. Wind apparatus to maximize the amount of kinetic energy associated with an air flow captured over time by said wind apparatus. UIBM IT 102022000019611, 23/03/2024. EPO, EP4343140 (A1), 27.03.2024. USPTO, US2024102451 (A1) Mar. 28, 2024
36. Anderson J. EBOOK: fundamentals of aerodynamics (SI units). New york: McGraw hill; 2011.
37. Vennell R. Exceeding the Betz limit with tidal turbines. Renew Energy. 2013;55:277–85.
38. Sørensen JN. General momentum theory for horizontal axis wind turbines, vol. 4. New York: Springer; 2016.
39. Van Kuik GAM, Lignarolo LE. M: Potential flow solutions for energy extracting actuator disc flows. Wind Energy. 2016;19(8):1391–406.
40. Bensalah A, Barakat G, Amara Y. Electrical generators for large wind turbine: trends and challenges. Energies. 2022;15(18):6700.
41. Beainy A, Maatouk C, Moubayed N, Kaddah F. Comparison of different types of generator for wind energy conversion system topologies. In: 2016 3rd International conference on renewable energies for developing countries (REDEC), pp. 1–6, Zouk Mosbeh, Lebanon (2016, July), 13–15 July 2016, https://doi.org/10.1109/REDEC.2016.7577535
42. Bumby JR, Stannard N, Dominy J, McLeod N. A permanent magnet generator for small scale wind and water turbines. In: 2008 18th International conference on electrical machines, Vilamoura, Portugal, 06–09 September 2008, pp. 1–6, https://doi.org/10.1109/ICELMACH.2008.4799855
43. Kebede AB, Worku GB, Maru AT. A novel train roof-top wind energy conversion system. Int J Eng Res Afr. 2022;61:165–94.
44. Sharma PK, Hari N, Banerjee S, Sharma R. A novel method of generating electricity by setting up turbines over rail locomotives. In: 2014 IEEE 6th India international conference on power electronics (IICPE), Kurukshetra, India, 08–10 December 2014, pp. 1–5 https://doi.org/10.1109/IICPE.2014.7115794
45. Dol LG, Cardassi JL, De Bernardinis A. Wind turbine for underground subway stations. In: PCIM Europe 2018; International exhibition and conference for power electronics, intelligent motion, renewable energy and energy management, pp. 1–6, Nuremberg, Germany, 05–07 June 2018
46. Menezes EJN, Araújo AM, Da Silva NSB. A review on wind turbine control and its associated methods. J Clean Prod. 2018;174:945–53.
47. Apata O, Oyedokun DTO. An overview of control techniques for wind turbine systems. Scient Afr. 2020;10: e00566.
48. Ghaffarzadeh H, Mehrizi-Sani A. Review of control techniques for wind energy systems. Energies. 2020;13(24):6666.
49. Chudzik S. Wind microturbine with adjustable blade pitch angle. Energies. 2023;16(2):945.
50. Njiri JG, Söffker D. State-of-the-art in wind turbine control: Trends and challenges. Renew Sustain Energy Rev. 2016;60:377–93.
51. Gambier, A. Overview of wind turbine control. In: Control of large wind energy systems. Advances in industrial control. Theory and methods for the user, 2022;95–106. Springer, Cham.
52. Navarrete EC, Perea MT, Correa JJ, Serrano RC, Moreno GR. Expert control systems implemented in a pitch control of wind turbine: A review. IEEE Access. 2019;7:13241–59.
53. Kane MB Machine learning control for floating offshore wind turbine individual blade pitch control. In: 2020 American control conference (ACC), Denver, CO, USA, 01–03 July 2020, pp. 237–241, https://doi.org/10.23919/ACC45564.2020.9147912
54. Kheirabadi AC, Nagamune R. A quantitative review of wind farm control with the objective of wind farm power maximization. J Wind Eng Ind Aerodyn. 2019;192:45–73.
55. Herbert-Acero JF, Probst O, Réthoré PE, Larsen GC, Castillo-Villar KK. A review of methodological approaches for the design and optimization of wind farms. Energies. 2014;7(11):6930–7016.
56. Slooff JW. The aero-and hydromechanics of keel yachts. Cham: Springer; 2015.
57. Sakhaei AH, Kaijima S, Lee TL, Tan YY, Dunn ML. Design and investigation of a multi-material compliant ratchet-like mechanism. Mech Mach Theory. 2018;121:184–97.